Identifying *in vivo* genetic dependencies of melanocyte and melanoma development

Sarah Perlee[1,2], Yilun Ma[1,3,4], Miranda V. Hunter[1], Jacob B. Swanson[5,6], Zhitao Ming[7], Julia Xia[1], Timothée Lionnet[5,6,8], Maura McGrail[7], Richard M. White[1,9,*]

[1]Department of Cancer Biology and Genetics, Memorial Sloan Kettering Cancer Center, New York, NY, USA
[2]Gerstner Sloan Kettering Graduate School of Biomedical Sciences, Memorial Sloan Kettering Cancer Center, New York, NY, USA.
[3]Weill Cornell/Rockefeller/Sloan Kettering Tri-Institutional MD-PhD Program, Memorial Sloan Kettering Cancer Center, New York, NY, USA.
[4]Cell and Developmental Biology Program, Weill Cornell Graduate School of Medical Sciences, New York, NY, USA.
[5]Institute for Systems Genetics, NYU Grossman School of Medicine, New York, NY, USA.
[6]Department of Cell Biology, NYU Grossman School of Medicine, New York, NY, USA.
[7]Department of Genetics, Development and Cell Biology, Iowa State University, IA, USA.
[8]Department of Biomedical Engineering, NYU Tandon School of Engineering, Brooklyn, NY.
[9]Nuffield Department of Medicine, Ludwig Institute for Cancer Research, University of Oxford, Oxford, UK.
[*] Correspondence to Richard M. White: Richard.white@ludwig.ox.ac.uk

Abstract

The advent of large-scale sequencing in both development and disease has identified large numbers of candidate genes that may be linked to important phenotypes. Validating the function of these candidates *in vivo* is challenging, due to low efficiency and low throughput of most model systems. We have developed a rapid, scalable system for assessing the role of candidate genes using zebrafish. We generated transgenic zebrafish in which Cas9 was knocked-in to the endogenous *mitfa* locus, a master transcription factor of the melanocyte lineage. We used this system to identify both cell-autonomous and non-cell autonomous regulators of normal melanocyte development. We then applied this to the melanoma setting to demonstrate that loss of genes required for melanocyte survival can paradoxically promote more aggressive phenotypes, highlighting that *in vitro* screens can mask *in vivo* phenotypes. Our high-efficiency genetic approach offers a versatile tool for exploring developmental processes and disease mechanisms that can readily be applied to other cell lineages.

Introduction:

Efficient cell type-specific knockout of genes is crucial for unraveling the intricate molecular mechanisms underlying cell function, development, and transformation. Zebrafish (*Danio rerio*) have emerged as a powerful genetic model organism for studying these processes. The large number of animals that can be easily generated make it advantageous (compared to other systems like mice) for querying large

numbers of genetic variants that may have links to human diseases. However, most studies in this system use germline knockout, which makes it difficult to determine whether the identified gene has a specific function in a particular lineage, or whether the phenotype reflects a more general developmental defect. Furthermore, many genes which might have lineage specific functions cannot be studied using germline knockout, since embryonic lethality often accompanies global knockout of essential genes[1]. To overcome these limitations, several groups have explored tissue-specific and conditional knockout strategies in zebrafish[2-10]. For example, the MAZERATI system uses tissue-specific promoter transgenes to drive Cas9 expression, which are introduced via plasmid injection into one-cell stage embryos[3,11]. Despite these advancements, efficiency remains of paramount importance. In normal development, low-efficiency knockout of a gene can mask important phenotypes, as the mutant cells can readily be outcompeted by wild-type or inframe mutations. Efficiency is even more important in the cancer context. Mutation of a tumor suppressor (i.e., PTEN) need not be highly efficient, since clones with a Darwinian advantage will inevitably outcompete other clones. However, in situations where we want to study necessity of a tumor promoting gene *in vivo* (i.e., an oncogene), cells which have mutations of a key driver gene will easily be outcompeted by nearby clones. Such efficiency is critical as sequencing projects such as All of Us, the UK Biobank and the Cancer DepMap continue to identify hundreds of new candidate genes on a regular basis, many of which have yet to be characterized *in vivo*[12-14].

Skin color pigmentation is amongst the most heterogeneous of genetic systems, with a large number of loci linked to melanocyte development. Mutations in pleiomorphic genes such as *sox10, ednrb, jam3b, tuba8l3, meox1* and *kit* yield clear defects in melanocyte/melanophore development, but these mutants also have defects in other tissues[15-21]. Many of these genes are also expressed in melanoma, but their specific *in vivo* function in tumorigenesis remains poorly understood.

In this study, we wished to develop a highly efficient and scalable system to understand *in vivo* genetic dependencies, using melanocytes and melanoma as an exemplar. By integrating the Cas9 nuclease into the endogenous melanocyte-specific *mitfa* locus, we achieved highly efficient and specific gene disruption across the melanocyte developmental lineage. We used our *mitfa*^{Cas9} knockin animals to inactivate the pigmentation gene *albino* and the embryonic essential genes *sox10, tuba1a,* and *ptena/b* in melanocytes without additional developmental or off-target phenotypes. We also demonstrated that this system can be used to efficiently induce melanomas in wild-type fish by inactivating the tumor suppressors *tp53* and *ptena/b* within melanocytes also expressing the melanoma oncogene BRAF^{V600E}. Inactivating the neural crest transcription factor *sox10* in these tumors significantly decreased melanoma initiation but resulted in rare invasive tumors that highly expressed the *sox9* transcription factor, highlighting that unexpected *in vivo* phenotypes can emerge that aren't predicted from *in vitro* studies[22,23]. Our system can thus be used to advance our understanding of melanocyte biology and the genetic underpinnings of phenotypic switching in melanoma, an approach that can readily be used for other cell types.

Results:

Targeted integration of Cas9 to the *mitfa* locus

To selectively disrupt genes in a melanocyte lineage-specific manner, we established a transgenic zebrafish line harboring Cas9 at the endogenous *mitfa* locus. *Mitfa* expression is detectable by 18 hours postfertilization (hpf) and is highly expressed in pigment cells including melanocytes, xanthophores and their progenitors. To achieve knock-in, we utilized the GeneWeld method, which enables efficient integration of DNA cassettes using homology mediated end joining (HMEJ)[24,25]. The knock-in cassette, containing Cas9 and BFP driven by the eye-specific γ-crystallin promoter, was targeted to exon 2 of the *mitfa* gene, which leads to disruption of the endogenous *mitfa* gene (Figure 1A). We strategically selected this genomic site for several reasons. First, this is the sole exon shared among the three *mitfa* protein-coding transcripts. Furthermore, targeting Cas9 to exon 2 offers the flexibility of replicating this knock-in strategy in *casper* zebrafish, a transparent fish widely used for melanoma studies that harbor a premature stop codon in *mitfa* exon 3[26].

The knock-in vector, along with Cas9 protein and guide RNAs targeting either the *mitfa* integration site or the sequences flanking the 5' and 3' homology arms, were injected into 1-cell stage wild-type Tropical 5D (T5D) zebrafish embryos (Figure 1B)[27]. An average of 19% of injected embryos had detectable ocular BFP expression at 3 days postfertilization (dpf), indicating successful integration (Figure S1A). Embryos were raised to adulthood then crossed with WT T5D fish. The resulting F1 embryos were screened for BFP+ eyes and tail clippings were sequenced to confirm precise integration of the knock-in cassette at the *mitfa* locus. We sequenced four F1 fish and detected on-target integration at the *mitfa* locus in all four fish (Figure S1B). In zebrafish, one copy of *mitfa* is sufficient for the normal development of neural crest-derived melanocytes, but loss of both copies of *mitfa* results in loss of the melanocyte lineage[26,28]. To determine the effect of a single copy of $mitfa^{Cas9}$ on melanocytes, $mitfa^{Cas9}$ fish were in-crossed and the resulting siblings were imaged at various time points (Figure S1C). WT and $mitfa^{Cas9}$ fish exhibited indistinguishable melanocyte patterning during both embryonic and adult stages. However, as expected, fish carrying two copies of Cas9 ($mitfa^{Cas9/Cas9}$) resembled the *nacre* mutant (*mitfa*-/-), characterized by complete loss of melanocytes, indicating the endogenous *mitfa* gene is disrupted on knock-in alleles[28]. We used zebrafish harboring one knock-in allele ($mitfa^{Cas9}$) for all subsequent experiments to allow us to test gene function in melanocytes.

To assess whether Cas9 expression was restricted to melanocytes, we performed fluorescence in situ hybridization (FISH) on 3dpf WT and $mitfa^{Cas9}$ embryos to measure *mitfa* and Cas9 mRNA expression (Figure 1C and S1D). In both WT and $mitfa^{Cas9}$ fish, *mitfa* was detected within the embryonic melanocyte stripe regions as expected. In $mitfa^{Cas9}$ fish, Cas9 mRNA was detected only within melanocyte stripe regions also expressing *mitfa*. These results provide functional validation for on-target integration and tissue-restricted expression of Cas9 to the melanocyte lineage.

Melanocyte-specific loss of the human skin color associated gene *slc45a2* results in robust loss of pigmentation

To assess the effectiveness of our stable *mitfa*^{Cas9} line, we first targeted the *albino* gene (*slc45a2*). Large scale GWAS studies have repeatedly identified SNPs in this gene as tightly linked to human skin color variation, and germline disruption leads to a complete loss of pigmentation in melanocytes[29-31]. This distinct phenotype enables the visual observation of Cas9 activity in zebrafish injected with *albino* gRNA. To test our system, we designed plasmids, denoted MG-gRNA, containing a zU6:gRNA cassette followed by *mitfa*:GFP to enable visualization of cells expressing the *albino* gRNA. MG-*albino* and MG-NT were injected into one-cell stage embryos from crosses between *mitfa*^{Cas9} and WT fish, which express Cas9 in all melanocytes but exhibit mosaic gRNA expression (Figure 2A).

Embryos were screened for BFP+ eyes to identify those harboring *mitfa*^{Cas9}. Upon adulthood, 92% of F0 MG-*albino* fish had mosaic loss of pigmentation within the melanocyte stripe regions (Figure 2B and C). Unpigmented regions maintained GFP expression (Figure 2B), indicating that the breaks in melanocyte stripes arise from loss of pigmentation in melanocytes rather than loss of the melanocyte lineage (Figure 2B). As expected, control MG-NT clutch mates displayed normal pigmentation and GFP+ melanocytes were indistinguishable from GFP- regions on the same fish (Figure 2B and C).

We next aimed to determine the efficiency of *mitfa*^{Cas9} in the F1 generation, in which every melanocyte stably expresses the *albino* gRNA and *mitfa*^{Cas9}. To generate F1 lines, we outcrossed the F0 MG-gRNA fish to WT and sorted embryos for BFP+ eyes and GFP+ melanocytes. F1 MG-*albino* fish exhibited a near complete loss of pigmentation, demonstrating that our *mitfa*^{Cas9} system is highly efficient in F1 fish (Figure 2D and E). To study the effect of *albino* inactivation across various stages of development, F1 MG-gRNA fish were once again outcrossed to WT, generating F2 MG-gRNA fish expressing one copy of *mitfa*^{Cas9}. Imaging revealed a measurable pigmentation loss in F2 MG-*albino* melanocytes as early as 3 days post-fertilization (dpf) (Figure 2F and G). F2 MG-*albino* fish maintained loss of pigmentation throughout development, indicating the sustained activity of *mitfa*^{Cas9} (Figure S2A-D).

To confirm on-target cutting of the *albino* gene in the melanocyte lineage (and not other tissues), the skin from F1 MG-*albino* fish was dissected and GFP+ and GFP- cells were isolated using FACS (Figure 2H). GFP+ cells encompass *mitfa*-expressing melanocytes, xanthophores, and their progenitors, while GFP- cells represent other non-melanocytic, non-*mitfa* expressing skin cells, such as keratinocytes, fibroblasts, and immune cells. We performed CRISPR-seq on DNA from both populations to directly measure Cas9 efficiency and specificity, quantifying the proportion of indels at the *albino* locus. Although we have previously shown that FACS sorting melanocytic cells is possible, it is important to note that we often observe high levels of contaminating keratinocytes in FACS sorted melanocyte populations, which may lead to an underestimation of the true allelic frequency in our CRISPR-seq[32]. Despite this, robust inactivation of the *albino* gene was observed in GFP+ (*mitfa*-expressing) cells, confirming somatic inactivation (Figure 2I). The majority of indels were frame-shift inducing mutations. A likely PCR or sequencing artifact resulting in a “T” insertion was

excluded from the frameshift indel percentage as it was observed in all conditions including WT fish with no pigmentation phenotype (Figure S2E). These results confirm that our *mitfa*^{Cas9} system allows us to inactivate genes within the melanocytic lineage *in vivo* in a highly efficient and specific manner.

The neural crest-related gene *sox10* has specific function in adult melanocyte patterning and regeneration

Having confirmed that our *mitfa*^{Cas9} system allows us to rapidly, efficiently and specifically manipulate melanocyte gene expression, we next wanted to target embryonic essential genes. Detecting "negative" gene knockout phenotypes such as cell death can be challenging *in vivo* due to the selective advantage that WT cells have over mutants. Current tissue specific knockout systems lack the sensitivity to detect negative phenotypes.

To assess the effectiveness of our *mitfa*^{Cas9} model in detecting negative phenotypes, we utilized it to target *sox10*, a transcription factor vital to the neural crest lineage and indispensable for overall survival of both zebrafish and mice[15,33]. Consequently, a global knockout approach is not feasible for studying the function of *sox10* in adult melanocytes *in vivo*. Germline knockout of *sox10* in zebrafish leads to severe defects in peripheral nerve development and the complete absence of melanocytes, and the animals die around day 14[15,34,35]. Due to the complete absence of melanocytes and their precursor cells, melanoblasts, in *sox10*$^{-/-}$ fish, it has not been possible to study the specific role of *sox10* on these more differentiated cell types *in vivo*. One of the key unanswered questions is how *sox10* balances its role in maintaining melanoblast stemness with promoting terminal differentiation, particularly in the context of adult melanocyte regeneration.

We leveraged our *mitfa*^{Cas9} system to specifically inactivate *sox10* in the melanocyte lineage. *mitfa*^{Cas9} fish injected with a MG-*sox10* plasmid exhibited noticeable gaps in their melanocyte stripes (Figure 3A-B). Germline deletion of a *sox10* enhancer region similarly affects adult stripe patterning in zebrafish[36]. In contrast to the *albino* F0 fish, the gaps in the stripes of the *sox10* F0 fish were not occupied by unpigmented GFP+ melanocytes, indicating a potential defect in the survival or differentiation of melanocytes upon loss of *sox10*. This phenotype became even more pronounced in the stable F1 lines, where several gaps are visible (Figure 3C). Zebrafish have four dark stripes occupied by melanocytes, which alternate with light colored interstripes occupied by yellow pigmented xanthophores[37]. Typically, melanocyte stripe 1D (dorsal) is wider than the interstripe X0 directly below it, as observed in MG-NT F1 fish (Figure 3C and D). However, the opposite is true for MG-*sox10* F1 fish, where we observed an apparent widening of the interstripe region and narrowing of the melanocyte stripes (Figure 3C and D). Melanocytes were counted in fish treated with epinephrine to aggregate melanosomes, revealing a significant reduction in the number of melanocytes in the F1 *sox10* KO fish compared to F1 NT fish (Figure 3E). Reduction in GFP+ cells within the xanthophore interstripes (X0) suggested that *sox10* deficiency also negatively affected xanthophore populations, in line with previous work indicating a role for *sox10* in specifying both xanthophores and melanocytes in zebrafish embryos[38].

Melanocytes continually regenerate throughout life, typically from a progenitor population of melanoblasts or melanocyte stem cells. We next assessed whether *sox10* was required for this. We treated adult fish with neocuproine, a copper chelator previously shown to kill mature, pigmented melanocytes[39]. We then compared regeneration from these progenitors in MG-*sox10* and MG-NT F1 fish by counting the percentage of melanocytes that emerged after 7, 15, and 70 days (Figure 3F). At days 7 and 15, when the melanocytes were still in the process of regenerating from melanoblasts, there were no significant differences between the two groups. However, by the time regeneration was completed we found a significant disparity between the regenerative potential of MG-NT and MG-*sox10* fish. At 70 days post-neocuproine treatment, MG-NT fish had regenerated an average of 82% of their melanocytes, whereas only 53% of melanocytes had regenerated in MG-*sox10* fish (Figures 3G-H). These findings demonstrate that *sox10* is required for adult melanocyte regeneration, highlighting its requirement within melanoblast populations outside of neural crest specification.

Non-autonomous functions of *tuba1a* on melanocytes

One of the significant challenges of conventional global knockout methods is the inability to differentiate between cell-autonomous and non-autonomous phenotypes. This distinction is particularly crucial in melanocyte studies due to their direct and indirect interactions with diverse cell types. A notable example of genes with pleiotropic effects is the tubulin gene family, whose α/β tubulin heterodimers form microtubules essential for various cellular processes such as cell division, motility, and intracellular transport across various cell types[40]. Microtubules are also critical for the transport of melanosomes in melanocytic cells[41].

Mutation of tubulin genes such as *tuba8l3a* in zebrafish leads to highly pleiotropic effects including defects in melanocyte patterning, CNS abnormalities, and altered craniofacial morphology[42]. We chose to focus on the closely related α tubulin gene *tuba1a*, which is highly expressed in many cell types of the developing zebrafish including melanocytes, but whose specific function in these cells remains unexplored[43]. Non-cell type specific knockout of *tuba1a* with the Alt-R CRISPR Cas9 system results in extensive embryo abnormalities including a curved tail phenotype, pericardial edema, and melanocytes with more dispersed pigmentation (Figure 4A-B, S3A-B). We found that compared to 71% survival of NT Alt-R embryos, only 10% of embryos injected with *tuba1a* Alt-R survive to 14dpf (Figure 4C).

Similar to *sox10,* the embryonic lethality of global *tuba1a* knockout prevents the study of knockout phenotypes in adult fish. To overcome this limitation, we implemented our *mitfa*^{Cas9} system to specifically knock out *tuba1a* in melanocytes. Unlike global knockout of *tuba1a*, melanocyte specific loss of *tuba1a* resulted in viable adult fish with no obvious abnormalities (Figure S3C-D). Surprisingly, we did not observe the dispersed melanocyte phenotype in any *mitfa*^{Cas9} MG-*tuba1a* embryos (Figure 4D, E). Based on this observation, we hypothesized that *tuba1a* may be functioning in a cell non-autonomous manner on melanocytes.

The dispersed pigmentation observed in *tuba1a* Alt-R embryos resembles that seen in blind zebrafish, which fail to contract their melanosomes in response to light[44]. This light-mediated camouflage involves retinal ganglion cells signaling hypothalamic neurons to release melanin-concentrating hormone (MCH), which then binds to MCH receptors on melanocytes, triggering melanosome aggregation via microtubules[44]. The normal melanosome dispersion observed in *mitfa*^{Cas9} MG-*tuba1a* fish suggests that rather than a cell-intrinsic defect in melanosome aggregation, *tuba1a* may indirectly influence melanocytes through potential defects in retinal and/or central nervous system cells crucial for light-mediated camouflage. Interestingly, TUBA1A mutation in humans can result in both ophthalmologic and brain abnormalities and morpholino-based knockdown of tuba1a in zebrafish inhibits CNS development[45,46].

To further test this idea, we treated *tuba1a* Alt-R embryos with epinephrine to assess their ability to contract melanosomes in response to a non-visual stimulus. *Tuba1a* Alt-R embryos exposed to epinephrine had robust aggregation of melanosomes, demonstrating that the loss of *tuba1a* did not impair melanosome transport (Figure 4F, G). This finding further supports a non-autonomous role for *tuba1a* in melanocytes. Utilizing the *mitfa*^{Cas9} system distinguish cell-autonomous from non-autonomous gene functions provides valuable insights into the complex dynamics of cell-cell interactions and how genes function within cellular and organismal networks.

Targeting tumor suppressors with *mitfa*^{Cas9} induces melanoma

We next turned our attention to melanoma. In humans, tumor suppressors such as *PTEN* and *TP53* are somatically inactivated in melanoma[47,48]. In contrast, the most commonly used zebrafish models of melanoma use a germline *tp53* mutation, which is not typically seen in humans with the disease and precludes our ability to discern the role of *tp53* inactivation specifically in melanocytes and melanoma[49]. While global *tp53* loss is not lethal, it does lead to a wide range of non-melanoma tumors, which can deteriorate fish health and confound melanoma studies[50]. Furthermore, current zebrafish melanoma models typically involve the utilization of MiniCoopR *mitfa* rescue cassettes into *casper* or *nacre* zebrafish, which are devoid of normal pigment cells. Although this method is highly efficient, it does not accurately represent melanoma initiation in the context of normal skin architecture and relies on artificial overexpression of *mitfa*. To mimic human melanoma initiation more accurately, we used our *mitfa*^{Cas9} model to assess tumor initiation using melanoma-specific gene knockout in animals with wild-type skin. Previous studies have shown that expression of BRAF^{V600E} and loss of *tp53* in WT (non-*casper*) fish results in relatively low tumor burden, so we decided to also target *ptena* and *ptenb*, the zebrafish orthologs of human *PTEN*[51]. *Ptena/ptenb* loss in combination with *tp53* has been shown to accelerate melanoma formation in zebrafish[52,53].

To first address the effect of *ptena/b* loss on normal melanocytes, we generated melanocyte-specific knockouts of *ptena* and *ptenb* (Figure 5A). Like *sox10* and *tuba1a*, germline knockout of *ptena/b* is embryonic lethal[54,55]. In our *ptena/ptenb* F0 melanocyte-specific KO fish, survival was normal. We observed an aberrant expansion of the

melanocytes outside of the stripe regions they normally are restrained to, suggesting that inactivation of *ptena* and *ptenb* induces defects in melanocyte patterning (Figure 5A and B). However, loss of *ptena/b* alone was not sufficient to induce melanoma.

To generate tumors, we co-injected *mitfa*^{Cas9} embryos with plasmids encoding *mitfa:*BRAF^{V600E} and sgRNAs targeting *tp53* and *ptena*/*b* (Figure 5C). Larvae were sorted for BFP+ eyes, indicating mitfa-Cas9 integration, and monitored for tumors over 30 weeks. No tumors were detected in BFP- fish from any of the injection conditions (n=136). We also did not observe any tumors in BFP+ fish injected with either BRAF^{V600E} alone (n=35) or ptena/b; *tp53* guides in the absence of BRAF^{V600E} (n=17). In contrast, tumors developed in all BFP+ groups injected with both *mitfa:*BRAF^{V600E} and gRNA plasmids. Approximately 5% of fish from the BRAF;*tp53* group developed tumors (Figure 5D). This aligns with a previous study where 6% of *tp53*-/- fish developed tumors when injected with a BRAF^{V600E} construct [51]. Targeting of *ptena* and *ptenb* in *mitfa*^{Cas9} fish co-injected with *mitfa*:BRAF^{V600E} resulted in a higher tumor incidence of 29% (Figure 5D).

When all three tumor suppressors (*tp53, ptena, ptenb*) were targeted in combination with BRAF^{V600E}, 59% of fish developed tumors by 30 weeks post fertilization (wpf) (Figure 5D). Immunohistochemistry (IHC) revealed that all tumor samples expressed BRAF^{V600E}, while p-AKT, a hallmark of *PTEN* inactivation, was only detected in samples with *ptena/b* KO (Figure 5E). To confirm on-target cutting, DNA was extracted from tumors and CRISPR sequencing was performed on PCR amplicons for each tumor suppressor gene. A large proportion of reads contained indels at the target locus for each of the target genes (*ptena*, *ptenb*, and *tp53*) (Figure 5F and S4). Some tumors had an array of mutations, while others appeared to be composed largely of a one dominant clone (Figure S4A to C). Our system thus allows us to rapidly dissect the melanocyte-specific function of both oncogenes (BRAF^{V600E}), as well as putative tumor suppressors (*tp53*, *ptena/b*), while avoiding pleiotropic effects of global tumor suppressor loss.

<u>Targeting of lineage-specific oncogenes decreases tumor initiation but promotes progression</u>

Our next objective was to leverage the mitfa^{Cas9} fish as a tool for identifying or validating potential genetic dependencies within melanoma. Genetic dependencies can be difficult to study *in vivo* since inactivation of a required gene inevitably leads to selection for non-mutant alleles, as has been previously shown[56]. In melanoma, the DepMap has identified *SOX10* as the top *in vitro* genetic dependency necessary for tumor cell proliferation, suggesting it acts as a lineage-specific oncogene[14,57]. In prior work in both zebrafish and mice, loss of *sox10* is clearly associated with a loss of tumor initiating potential and cell proliferation[56,57]. Yet its specific role *in vivo* remains unclear, since it is required for neural crest and melanocyte specification, making it difficult to know whether its effects reflect loss of the entire lineage[57]. Given our data above showing that *sox10* is required specifically in melanocyte patterning and regeneration, we wished to investigate its function in melanoma.

368 To assess this, we generated plasmids containing multiple sgRNAs driven by three
369 distinct zU6 promoters (zU6A, zU6B, and zU6C) to simultaneously target both tumor
370 suppressors (*tp53, ptena/ptenb*) and tumor promoting genes (*sox10*) in the same cells,
371 which reduces the chance of selecting for non-mutant alleles[2]. We co-injected these
372 plasmids with *mitfa*:BRAF^{V600E}, sorted fish for BFP+ eyes, and tracked tumor free
373 survival over the course of 50 weeks (Figure 6A and B). Consistent with the DepMap
374 prediction, *sox10* inactivation markedly reduced tumor incidence, which likely reflects
375 loss of proliferation. Only 3/96 (3.1%) fish with *sox10* knockouts initiated melanomas
376 compared to the 24/94 fish (25.5%) from the NT condition that developed tumors
377 (Figure 6B). Using IHC, we validated that *sox10* KO tumors expressed lower levels of
378 Sox10 protein compared to NT tumors (Figure 6C and S5A). Quantification of Sox10
379 intensity with immunofluorescence confirmed this finding (Figure S5B).
380
381 Although *sox10* clearly reduced tumor initiation, we noted "escapers". These tumors
382 appeared morphologically very distinct compared to the *sox10* intact tumors.
383 Specifically, these tumors were highly invasive with a mesenchymal morphology
384 compared to the typical BRAF^{V600E} melanoma (Figure 6C). This observation raised the
385 possibility that these tumors had undergone "phenotype switching", a form of cell
386 plasticity in which cells reversibly move between opposite extremes of proliferation
387 versus invasive states[22,23,57,58]. In melanoma, the proliferative state is thought to be
388 characterized by high expression of *SOX10*, whereas the mesenchymal, invasive state
389 is characterized by high expression of *SOX9*[23]. These two highly related transcription
390 factors have seemingly opposite and possibly antagonistic roles in melanoma. *In vitro*,
391 knockout of *SOX10* in a variety of human cell lines is associated with acquisition of a
392 *SOX9*^{hi} state, which has been suggested to be linked to the invasive phenotype[23]. Re-
393 analysis of publicly available RNA-seq data using 3 patient-derived human melanoma
394 cell lines treated with siRNA targeting *SOX10* confirmed this observation, with the
395 *SOX10* lines now becoming *SOX9*^{hi} (Figure 6E to J, S5C to L)[23]. These data raised the
396 hypothesis that the more invasive tumors we see in our escaper fish was due to gain of
397 *sox9* expression. To test this, we stained our *sox10* CRISPR tumors for *sox9* and
398 discovered that 2 of the 3 *sox10* KO tumors markedly upregulated *sox9* relative to
399 control tumors expressing NT gRNA (Figure 6C and D). This data highlights that *in vitro*
400 genetic studies such as the DepMap, which rely on proliferation as the readout, can
401 mask more complex *in vivo* phenotypes.
402
403 **Discussion:**
404 The ability to model genetic dependencies *in vivo* is one of the most important uses of
405 model organisms. Forward genetic mutagenesis screens using compounds such as
406 ENU or EMS led to the identification of many key developmental genes in organisms
407 such as Drosophila, C. elegans, Saccharomyces, zebrafish, and many others[59,60].
408 These approaches have rapidly accelerated in the era of TALENs and CRISPR, readily
409 allowing for knockout of nearly any gene in a wide variety of non-model organisms.
410 Cre/Lox approaches have further augmented our ability to discern the cell-type specific
411 effects of these genes, although these are still laborious and time consuming, especially
412 in models such as mice[10].
413

414 Alongside these approaches have been remarkable advances in large scale sequencing
415 of human tissues. GWAS-like efforts such as the UK Biobank and the US All of Us
416 programs have identified thousands of germline variants (SNPs) that may be linked to
417 interesting phenotype variation[12,13]. A conceptually similar approach is also happening
418 in diseases such as cancer, in which efforts such as the TCGA, ICGC and DepMap
419 have continued to unveil new potential somatic variants (SNVs) linked to cancer[14,61,62].
420
421 Across these efforts, in both development and disease, the large number of candidate
422 variants makes it challenging to connect these genotypes to phenotypes. This is
423 especially acute in melanoma, where the large number of somatic variants generated by
424 UV radiation leads to a high number of background mutations that may or may not have
425 pathogenic function. Thus, there is a substantial need for *in vivo* models that allow for
426 rapid and efficient modeling of candidate genes. Our development of the *mitfa*-Cas9
427 knockin line provides such a method. One major advantage is that phenotypes can be
428 readily screened either in the F0 generation (as mosaics) or in the F1 generation (3
429 months later). The F1 fish in particular are advantageous, since they allow for highly
430 efficient biallelic knockout of the gene of interest, allowing for very quick identification of
431 genes that only have recessive phenotypes (i.e., *albino*). On a per gene basis, this
432 saves well over 3 months of work compared to germline knockouts and uses vastly
433 fewer animals since all F1 animals (even those for recessive alleles) are informative.
434 Additionally, this model eliminates the issue of inbreeding, promoting healthier genetic
435 lines and facilitating the potential for outcrossing with any available fish line. Because
436 we demonstrate that the Cas9 is completely restricted to the melanocyte lineage, with
437 no detectable off-target expression, this easily allows us to discern the melanocyte-
438 specific effect of pleiotropic genes very efficiently.
439
440 One interesting observation of our melanoma studies is evidence that loss of melanoma
441 genetic dependencies like *SOX10* (as suggested by the human DepMap data) can still
442 lead to tumors, albeit with very different biological behaviors. In both the fish and in the
443 human samples we analyzed, loss of *SOX10* leads to acquisition of a *SOX9*^{hi} state
444 instead[23]. *SOX9* is increasingly recognized to be a potent mediator of tumor cell
445 invasiveness, which is what we observe in our fish[63,64]. One implication of this finding is
446 that clinical targeting of transcription factors like *SOX10*, long considered an ideal
447 therapeutic approach, could lead to unexpected outcomes in which tumors might
448 proliferate less but become more invasive or resistant to therapy. Whether this
449 phenomenon of *SOX10/SOX9* switching is a general phenomenon, or specific to that
450 class of TFs, remains to be determined. However, a similar phenomenon has been
451 observed for *MITF*, another melanocytic TF, suggesting this idea of TF switching needs
452 to be more thoroughly explored in the future[58,65,66].
453
454 Finally, while our studies clearly focused on the melanocyte lineage, highly similar
455 approaches could be taken for virtually any cellular lineage in which master regulators
456 or markers are known. Given the large number of already identified promoter/enhancer
457 fragments in the zebrafish, this would be an important extension of our system to study
458 gene variants in the context of development and other diseases[67].
459

Our approach has several limitations that may need to be addressed in future studies. Due to the constitutive nature of the Cas9, we have little control over the timing of its expression. Because it is knocked into the endogenous *mitfa* locus, the expression of Cas9 will vary with the endogenous regulation of that gene. In future iterations of this general approach, swapping the Cas9 for an inducible version would allow for better timed knockout of genes[68]. Because *mitfa* itself is expressed in melanoblasts, melanophores and xanthophores during different stages of development, choosing a promoter (e.g. PMEL) that is more tightly restricted to melanocytes may be advantageous. Finally, although our system was relatively efficient, we still did not see 100% knockout. This may reflect that it is relatively easy to bypass the CRISPR lesion in an exon with an in-frame mutation. The use of multiple sgRNAs, or sgRNAs that target promoter regions, rather than exons, could further augment efficiency of knockout. Alternatively, instead of targeting DNA, we could consider using RNA targeting CRISPR enzymes. Recent work has shown that RNA degradation induced by Cas13 works in zebrafish and may allow for more nuanced knockdown rather than knockout of a given candidate gene[69,70]. This may especially have advantages in the context of melanoma, where genes are commonly dysregulated rather than completely knocked out. We envision it would be relatively straightforward to knock Cas13 into the locus of interest using an analogous approach to the one we have taken here.

Acknowledgements:
We thank members of the White lab for valuable discussions and feedback on this project. We thank Nelly Cruz Esteves for helpful feedback on the manuscript. We also thank the MSKCC flow cytometry core for assistance with cell sorting, Integrated Genomics Operation Core, funded by an NCI Cancer Center Support Grant (P30 CA08748) for sequencing assistance, and Molecular Cytology Core for their help with imaging. We thank the MSKCC aquatics core facility for their support of this work. Schematic figures were all made using Biorender.com with a paid Biorender license.

Funding:
RMW was funded through the NIH/NCI Cancer Center Support Grant P30 CA008748, the Melanoma Research Alliance, The Debra and Leon Black Family Foundation, NIH Research Program Grants R01CA229215 and R01CA238317, NIH Director's New Innovator Award DP2CA186572, The Pershing Square Sohn Foundation, The Mark Foundation for Cancer Research, The American Cancer Society, The Alan and Sandra Gerry Metastasis Research Initiative at the Memorial Sloan Kettering Cancer Center, The Harry J. Lloyd Foundation, Consano and the Starr Cancer Consortium. This work was also supported by NIH ORIP R24OD020166 (MM). YM was supported by a Medical Scientist Training Program grant from the NIH under award number T32GM007739 to the Weill Cornell/Rockefeller/Sloan Kettering Tri-Institutional MD-PhD Program and Kirschstein-National Research Service Award (NRSA) predoctoral fellowship under award number F30CA265124. MVH was funded by a K99/R00 Pathway to Independence Award from the National Cancer Institute (1K99CA266931). SP was funded by a Molecular Imaging in Cancer Biology Training Grant at Memorial Sloan Kettering Cancer Center from the National Cancer institute (T32CA254875) and the

Ruth L. Kirschstein National Research Service Award for Individual Predoctoral Fellows from the National Cancer Institute (F31CA271518).

Author Contributions:

Conceptualization: SP, RMW
Investigation: SP, YM, MVH, JBS, ZM, JX
Visualization: SP, MVH, JBS
Supervision: TL, MM, RMW
Writing—original draft: SP, RMW
Writing—review & editing: SP, MVH, RMW

Declaration of Interests:

MM has competing interests with Recombinetics Inc., LifEngine Technologies, and LifEngine Animal Health Laboratories, Inc. RMW is a paid consultant to N-of-One Therapeutics, a subsidiary of Qiagen and is on the scientific advisory board of Consano but receives no income for this. RMW receives royalty payments for the use of the *casper* zebrafish line from Carolina Biologicals. SP, YM, MVH, JBS, ZM, JX, and TL declare no competing interests.

Methods

Materials Availability: All data are available in the main text or the supplementary materials, or upon request. Plasmids, fish lines and other materials generated from this study are available upon request.

Zebrafish husbandry and ethics statement

All zebrafish experiments adhered to institutional animal protocols and were conducted in compliance with approved procedures. Fish stocks were maintained at a temperature of 28.5 °C, under 14:10 light:dark cycles, with pH set at 7.4, and salinity-controlled conditions. The zebrafish were fed a standard diet comprising brine shrimp followed by Zeigler pellets. Approval for the animal protocols outlined in this manuscript was obtained from the Memorial Sloan Kettering Cancer Center (MSKCC) Institutional Animal Care and Use Committee (IACUC), under protocol number 12-05-008. Anesthesia was conducted using Tricaine (4 g/l, Syndel, Ferndale, WA, USA) from a stock of 4 g/l and diluted to 0.16 mg/ml. Adult zebrafish of both sexes were equally employed in all experiments. Embryos, collected through natural mating, were incubated in E3 buffer (5 mM NaCl, 0.17 mM KCl, 0.33 mM CaCl2, 0.33 mM MgSO4) at 28.5 °C. The wild-type strain used was Tropical 5D Zebrafish (T5D)[27].

GeneWeld plasmid construction

A combination of restriction enzyme digestion and HiFi cloning was used to construct the GeneWeld pPRISM-nCas9n, γcry1:BFP vector for targeted integration to isolate an nls-Cas9-nls knockin. A 765 bp fragment containing the Porcine teschovirus-1 polyprotein 2A peptide sequence was amplified from the pPRISM-2A-Cre, γcry1:BFP vector (Addgene #117789) with primers Ori-F and 2A-R[24,25]. The nCas9n cDNA was

551 amplified from the expression vector pT3TS-nCas9n (Addgene #46757) with primers
552 Cas9-F and Cas9-R[71]. A KpnI/SpeI fragment containing the pPRISM-2A-Cre, gcry1:BFP
553 vector backbone was assembled with the 2A and nCas9n PCR amplicons using the
554 NEBuilder HiFi DNA Assembly Cloning Kit (NEB # E5520S) following the
555 manufacturer's instructions.
556
557 Homology arms were designed as previously described[24,25]. Briefly, 48bp homology
558 arms complementary to the *mitfa* target site were designed using GTagHD
559 (http://www.genesculpt.org/gtaghd/) for the pPRISM GeneWeld plasmid series. The two
560 pairs of complementary oligos can be found in Table S1. 5' and 3' arms were cloned
561 sequentially into the pPRISM-nCas9n, γcry1:BFP vector. The 3' homology arm oligos
562 were annealed and cloned into the vector using the BspQI restriction site as previously
563 described. Due to the multiple BfuAI sites within Cas9, instead of using BfuAI restriction
564 cloning, we alternatively used in-fusion cloning (Takara Bio) to insert a gBlock (IDT)
565 containing the 5' homology arm into the pPRISM-nCas9n, gcry1:BFP vector. Primers
566 and gblock sequence used for cloning are listed in Table S1. The 5' and 3' homology
567 arms were sequenced with primers 5'homologycheckF and R3'_pgtag_seq,
568 respectively.
569
570 **Injection of GeneWeld reagents**
571 Injections of GeneWeld reagents were performed on one-cell stage embryos. We used
572 the Alt-R CRISPR-Cas9 system (IDT) for the initial knock-in of nCas9n, γcry1:BFP to
573 the *mitfa* locus. In brief, 100 µM tracrRNA (IDT 1075928) was mixed at a 1:1 ratio with
574 either *mitfa* crRNA or universal crRNA then incubated at 95 °C for 5 min. Recombinant
575 Cas9 (IDT 1081059) was incubated with both sgRNAs for 10 min at 37 °C to form the
576 RNP complex. The GeneWeld pPRISM-5'mitfaHom-nCas9n, gcry1:BFP-3'mitfaHom
577 plasmid was then added to the injection mix along with phenol red (Sigma-Aldrich
578 P0290) . The final concentrations injected into the embryos were: 75 pg/nl Cas9, 12.5
579 pg/nl *mitfa* sgRNA, 12.5 pg/nl Universal sgRNA, and 5 pg/nl pPRISM plasmid.
580
581 **Genotyping**
582 Tail clips were taken from 2 month postfertilization (mpf) zebrafish and DNA was
583 extracted using the DNeasy Blood and tissue kit (Qiagen). DNA was PCR amplified with
584 Q5 high fidelity DNA polymerase (NEB). The forward primer MitfaPCR-F binds to the
585 *mitfa* genomic region upstream of the insertion site and the reverse primer
586 5'homology_amplify-R binds the p2A region of the insertion cassette. Expected PCR
587 amplicon size is 269bp. Amplicons were sequenced using sanger sequencing (Azenta
588 Life Sciences).
589
590 **RNA-FISH HCR**
591 We adapted the HCR protocol from Ibarra-Garcia-Padilla et al.[72]. Briefly, embryos were
592 collected and treated with 0.0045% 1-phenyl 2-thiourea (PTU) (Sigma-Aldrich) after 24
593 hpf to block pigmentation. Embryos were harvested at 72 hpf and fixed in 4% PFA
594 (Santa Cruz) for 24 hrs at 4 °C. Embryos were then washed with PBS and
595 dehydrated/permeabilized with a series of MeOH (Millipore) washes. Embryos were
596 rehydrated with a series of MeOH/PBST washes, permeabilized with acetone (Fisher

Scientific) and incubated with Proteinase K (Millipore) for 30 min. This was followed by further fixation with 4% PFA. Embryos were pre-hybridized in probe hybridization buffer (PHB) before incubating them with HCR probes in PHB at concentration of 20nM. Probe sequences for *mitfa* and Cas9 can be found in Table S1. Embryos were washed with probe wash buffer before being pre-amplified with probe amplification buffer (PAB). Following pre-amplification, amplifier hairpins were thawed, snap-cooled, and mixed with PAB to a concentration of 36 nM. Embryos were incubated in the hairpin solution followed by washes with 5×SSCT and 1× PBST. Embryos were stained with 2 µg/mL DAPI in PBST and mounted on glass slides. Imaging was performed using a Zeiss LSM880 confocal microscope.

Guide RNA plasmids

The following plasmids were constructed using the Gateway Tol2kit:
zU6A:gRNA-NT;zU6B:gRNA-*ptena*;zU6C:gRNA-*tp53*/394,
zU6A:gRNA-NT;zU6B:gRNA-*ptenb*;zU6C:gRNA-*tp53*/394,
zU6A:gRNA-*sox10*;zU6B:gRNA-*ptena*;zU6C:gRNA-*tp53*/394,
zU6A:gRNA-*sox10*;zU6B:gRNA-*ptenb*;zU6C:gRNA-*tp53*/394.

In-fusion cloning (Takara Bio) was used to insert *mitfa:*GFP or *mitfa:*TdTomato into a zU6:gRNA/394 plasmid previously developed in the lab (See Table S1 for primers used). gRNAs were cloned into zU6:gRNA;*mitfa:*GFP/394 or zU6:gRNA;*mitfa:*TdTomato/394 using BsmBI sites. Other plasmids used in this study that were previously developed in the lab include zU6:gRNA-*ptena*/394, zU6:gRNA-*ptenb*/394, zU6:gRNA-*tp53*/394, *mitfa*-BRAF^{V600E};cmlc2:eGFP. All guide RNAs used in this study besides *tuba1a* have previously been validated in zebrafish[24,32,56,73].

Validation of *tuba1a* sgRNA

The Alt-R CRISPR-Cas9 system (IDT) was used to achieve non-cell type specific knockout of *tuba1a.* Guide RNAs were designed using ChopChop[74]. In brief, 100 µM tracrRNA (IDT 1075928) was mixed at a 1:1 ratio with *tuba1a* crRNA then incubated at 95 °C for 5 min. Recombinant Cas9 (IDT 1081059) was incubated with the *tuba1a* sgRNA for 10 min at 37 °C to form the RNP complex. Phenol red was added prior to injection into 1 cell-stage wild-type T5D embryos. To validate on-target cutting, 4 embryos were pooled and DNA was extracted using Quick Extract buffer (Fisher Scientific NC0302740). DNA was PCR amplified with Q5 high fidelity DNA polymerase (NEB) and primers tuba1a_seq-F and tuba1a_seq-R. Exosap IT for PCR Product Clean Up was added to PCR product prior to sanger sequencing. Primers tuba1a_seq-F and tuba1a_seq-R were also used for sequencing.

Transgenic lines

To generate MG-U6:sgRNA stable lines, one-cell-stage embryos from crossing WT and mitfa:Cas9 fish were collected and injected with the 30 pg indicated plasmid and 20 pg tol2 mRNA. Fish with GFP+ melanocytes and BFP+ eyes were selected and outcrossed with WT fish to produce the F1 generation. F1 fish were again sorted and outcrossed to generate F2 generation zebrafish. All fish were imaged on a Zeiss AxioZoom V16 with Zen 2.1 software.

643
644 **Flow cytometry of melanocytes from adult zebrafish**
645 Zebrafish were euthanized using ice-cold water and dissected using a clean scalpel and
646 forceps. The epidermal and dermal layers of the skin as well as the fins were separated
647 from the rest of the tissues and diced into 1-3mm pieces. Cells were dissociated with
648 Liberase TL (Millipore Sigma 05401020001) and filtered for single cell suspensions as
649 previously described[32]. Samples were then FACS sorted (BD FACSAria) for GFP+ and
650 GFP- cells. WT fish were used as a GFP negative control. Genomic DNA was isolated
651 from sorted cells using the DNeasy Blood and Tissue Kit (Qiagen).
652
653 **Tumor Dissection**
654 Fish with tumors were euthanized with ice-cold water and immediately dissected with a
655 scalpel to isolate tumor tissue. Genomic DNA was purified from the tumor samples
656 using the Dneasy Blood and tissue kit (Qiagen).
657
658 **CRISPR sequencing**
659 Primer pairs were designed to produce amplicons 200 to 280 bp in length with the
660 mutation site within 100 bp from the beginning or end of amplicon (see Table S1 for
661 primer sequences). Genomic DNA isolated from methods detailed above was PCR
662 amplified with Q5 high fidelity DNA polymerase (NEB) and run on an agarose gel to
663 visualize PCR products. The samples were then purified using the NucleoSpin Gel and
664 PCR cleanup kit (Takara Bio). Deep sequencing was conducted using the CRISPR-seq
665 platform. Sequencing data was analyzed with CRISPResso2[75]. and indel charts were
666 generated with CRISPRVariants R package[76].
667
668 **Drug treatments**
669 Adult zebrafish were treated for 24 hr with 750nM neocuproine (Sigma-Aldrich)
670 dissolved in fish water with a final concentration of 0.0075% DMSO as previously
671 described [39]. Cells from the middle melanocyte stripe were counted within a rectangular
672 region of 4mm x 1.5mm. Epinephrine hydrochloride (Sigma-Aldrich) was used at 1
673 mg/ml in fish water. Fish were treated for 10 minutes prior to imaging.
674
675 **Zebrafish tumor-free survival curves**
676 To generate a transgenic melanoma model, one-cell-stage embryos from WT X
677 mitfa:Cas9 fish crosses were injected with *mitfa*-BRAF^{V600E};cmlc2:eGFP, 20 pg Tol2
678 mRNA, and the indicated gRNA plasmids for each condition. The total amount of
679 plasmid per embryo did not exceed 30 pg. Embryos were screened for GFP positive
680 hearts and sorted for BFP+ or BFP- eyes. Fish were screened for tumors using a
681 microscope every 2 weeks starting at 4 weeks post fertilization. Tumors were only
682 called if an elevated lesion was observed. Graphpad prism 9 was used to generate and
683 analyze Kaplan-Meier survival curves. Statistical differences were determined using log-
684 rank Mantel–Cox test. All screening and imaging was conducted on a Zeiss AxioZoom
685 V16 using Zen 2.1 software.
686
687 **Histology**

688 Zebrafish were sacrificed using ice-cold water and placed in 4% paraformaldehyde
689 (Santa Cruz 30525-89-4) in PBS for 72 h at 4°C on a rocker. Fish were then transferred
690 to 70% EtOH for 24 h at 4°C on a rocker. Fish were sent to Histowiz, Inc (Brooklyn, NY,
691 USA), where they were paraffin embedded, sectioned, stained and imaged. All the
692 stainings were performed at Histowiz, Inc Brooklyn, using the Leica Bond RX automated
693 stainer (Leica Microsystems) using a Standard Operating Procedure and fully
694 automated workflow. Samples were processed, embedded in paraffin, and sectioned at
695 4µm. The slides were dewaxed using xylene and alcohol based dewaxing solutions.
696 Epitope retrieval was performed by heat-induced epitope retrieval (HIER) of the
697 formalin-fixed, paraffin-embedded tissue using Citrate based pH 6 solution (Leica
698 Microsystems, AR9961) for 20 mins at 95 C. The tissues were first incubated with
699 peroxide block buffer (Leica Microsystems), followed by incubation with the following
700 antibodies for 30 min: BRAFV600E antibody (ab228461, 1:100), phospho-AKT antibody
701 (CST4060, 1:50), SOX9 antibody (AB_185230, 1:1000), and SOX10 antibody
702 (GTX128374, 1:500). This was followed by incubation with DAB secondary reagents:
703 polymer, DAB refine and hematoxylin (Bond Polymer Refine Detection Kit, Leica
704 Microsystems) according to the manufacturer's protocol. The slides were dried,
705 coverslipped (TissueTek-Prisma Coverslipper) and visualized using a Leica Aperio AT2
706 slide scanner (Leica Microsystems) at 40X.
707
708
709 **Quantification of Sox10 intensity**
710 FFPE slides were deparaffinized by consecutive incubations in xylene and 100-50%
711 ethanol. For antigen retrieval, slides were placed in 10 mM sodium citrate pH 6.2 in a
712 pressure cooker and heated to 95°C for 20 minutes. Slides were then cooled to room
713 temperature and blocked in 5% donkey serum, 1% BSA, and 0.4% Triton-X100 in PBS
714 for 1 hour at room temperature. The primary antibody targeting Sox10 (GeneTex,
715 GTX128374) was added to the blocking buffer at 1:200 concentration and incubated at
716 4°C overnight. Slides were then washed in PBS before incubation with the secondary
717 antibody (donkey anti-rabbit Alexa Fluor Plus 488, Thermo Fisher Scientific #AC32790;
718 1:250) and Hoescht (Thermo Fisher Scientific, #62249; 1:1000) in blocking buffer for 2
719 hours at room temperature. Slides were mounted in Vectashield Plus (Vector Labs, H-
720 1900). Slides were imaged on a LSM 880 confocal microscope using a 40X oil
721 immersion objective. 3 images were captured per sample. Quantification of Sox10
722 intensity per cell was performed using CellProfiler.[77] and MATLAB r2023b (Mathworks).
723 Cells were segmented in CellProfiler to obtain a nuclear mask from the Hoescht signal
724 and using this mask the mean intensity per nucleus was quantified.
725
726 **Re-analysis of human melanoma scRNA-seq data**
727 Human melanoma scRNA-seq data from Wouters et al. was accessed from GEO
728 (GSE134432)[23]. All analysis was done in R (version 4.3.1) using the Seurat package
729 (version 5.0.2)[78]. Counts matrices for each sample and cell line were imported into R
730 and converted into Seurat objects before merging into one combined Seurat object.
731 Counts were normalized using the Seurat function NormalizeData with default
732 parameters. UMAP was calculated using the Seurat function RunUMAP with 10
733 dimensions.

Statistical analysis

Statistical significance was analyzed using t test, Log-rank (Mantel-Cox) test, Wilcoxon Rank Sum Test or as indicated in the figure legends. GraphPad Prism 9 software was used for data processing and statistical analysis. *P < 0.05; **P < 0.005; ***P < 0.001; ****P < 0.0001. Data are presented as means ± SD unless otherwise indicated.

References

1. Amsterdam, A. *et al.* Identification of 315 genes essential for early zebrafish development. *Proc Natl Acad Sci U S A* **101**, 12792-7 (2004).
2. Yin, L. *et al.* Multiplex Conditional Mutagenesis Using Transgenic Expression of Cas9 and sgRNAs. *Genetics* **200**, 431-41 (2015).
3. Ablain, J., Durand, E.M., Yang, S., Zhou, Y. & Zon, L.I. A CRISPR/Cas9 vector system for tissue-specific gene disruption in zebrafish. *Dev Cell* **32**, 756-64 (2015).
4. Zhou, W. *et al.* Neutrophil-specific knockout demonstrates a role for mitochondria in regulating neutrophil motility in zebrafish. *Dis Model Mech* **11**(2018).
5. Ni, T.T. *et al.* Conditional control of gene function by an invertible gene trap in zebrafish. *Proc Natl Acad Sci U S A* **109**, 15389-94 (2012).
6. Grajevskaja, V., Camerota, D., Bellipanni, G., Balciuniene, J. & Balciunas, D. Analysis of a conditional gene trap reveals that tbx5a is required for heart regeneration in zebrafish. *PLoS One* **13**, e0197293 (2018).
7. Burg, L. *et al.* Conditional mutagenesis by oligonucleotide-mediated integration of loxP sites in zebrafish. *PLoS Genet* **14**, e1007754 (2018).
8. Kalvaityte, M. & Balciunas, D. Conditional mutagenesis strategies in zebrafish. *Trends Genet* **38**, 856-868 (2022).
9. Singh Angom, R., Wang, Y., Wang, E., Dutta, S.K. & Mukhopadhyay, D. Conditional, Tissue-Specific CRISPR/Cas9 Vector System in Zebrafish Reveals the Role of Nrp1b in Heart Regeneration. *Arterioscler Thromb Vasc Biol* **43**, 1921-1934 (2023).
10. Shin, M. *et al.* Generation and application of endogenously floxed alleles for cell-specific knockout in zebrafish. *Dev Cell* **58**, 2614-2626 e7 (2023).
11. Ablain, J., Liu, S., Moriceau, G., Lo, R.S. & Zon, L.I. SPRED1 deletion confers resistance to MAPK inhibition in melanoma. *J Exp Med* **218**(2021).
12. Mayer, C.S. & Huser, V. Learning important common data elements from shared study data: The All of Us program analysis. *PLoS One* **18**, e0283601 (2023).
13. Sudlow, C. *et al.* UK biobank: an open access resource for identifying the causes of a wide range of complex diseases of middle and old age. *PLoS Med* **12**, e1001779 (2015).
14. Tsherniak, A. *et al.* Defining a Cancer Dependency Map. *Cell* **170**, 564-576 e16 (2017).
15. Dutton, K.A. *et al.* Zebrafish colourless encodes sox10 and specifies non-ectomesenchymal neural crest fates. *Development* **128**, 4113-25 (2001).
16. Parichy, D.M. *et al.* Mutational analysis of endothelin receptor b1 (rose) during neural crest and pigment pattern development in the zebrafish Danio rerio. *Dev Biol* **227**, 294-306 (2000).

780 17. Eom, D.S., Patterson, L.B., Bostic, R.R. & Parichy, D.M. Immunoglobulin
781 superfamily receptor Junctional adhesion molecule 3 (Jam3) requirement for
782 melanophore survival and patterning during formation of zebrafish stripes. *Dev*
783 *Biol* **476**, 314-327 (2021).
784 18. Parichy, D.M. & Turner, J.M. Zebrafish puma mutant decouples pigment pattern
785 and somatic metamorphosis. *Dev Biol* **256**, 242-57 (2003).
786 19. Nguyen, P.D. *et al.* Haematopoietic stem cell induction by somite-derived
787 endothelial cells controlled by meox1. *Nature* **512**, 314-8 (2014).
788 20. Irion, U., Singh, A.P. & Nusslein-Volhard, C. The Developmental Genetics of
789 Vertebrate Color Pattern Formation: Lessons from Zebrafish. *Curr Top Dev Biol*
790 **117**, 141-69 (2016).
791 21. Parichy, D.M., Rawls, J.F., Pratt, S.J., Whitfield, T.T. & Johnson, S.L. Zebrafish
792 sparse corresponds to an orthologue of c-kit and is required for the
793 morphogenesis of a subpopulation of melanocytes, but is not essential for
794 hematopoiesis or primordial germ cell development. *Development* **126**, 3425-36
795 (1999).
796 22. Capparelli, C. *et al.* Targeting SOX10-deficient cells to reduce the dormant-
797 invasive phenotype state in melanoma. *Nat Commun* **13**, 1381 (2022).
798 23. Wouters, J. *et al.* Robust gene expression programs underlie recurrent cell states
799 and phenotype switching in melanoma. *Nat Cell Biol* **22**, 986-998 (2020).
800 24. Welker, J.M. *et al.* GeneWeld: Efficient Targeted Integration Directed by Short
801 Homology in Zebrafish. *Bio Protoc* **11**, e4100 (2021).
802 25. Wierson, W.A. *et al.* Efficient targeted integration directed by short homology in
803 zebrafish and mammalian cells. *Elife* **9**(2020).
804 26. White, R.M. *et al.* Transparent adult zebrafish as a tool for in vivo transplantation
805 analysis. *Cell Stem Cell* **2**, 183-9 (2008).
806 27. Balik-Meisner, M., Truong, L., Scholl, E.H., Tanguay, R.L. & Reif, D.M.
807 Population genetic diversity in zebrafish lines. *Mamm Genome* **29**, 90-100
808 (2018).
809 28. Lister, J.A., Robertson, C.P., Lepage, T., Johnson, S.L. & Raible, D.W. nacre
810 encodes a zebrafish microphthalmia-related protein that regulates neural-crest-
811 derived pigment cell fate. *Development* **126**, 3757-67 (1999).
812 29. Fernandez, L.P. *et al.* SLC45A2: a novel malignant melanoma-associated gene.
813 *Hum Mutat* **29**, 1161-7 (2008).
814 30. Branicki, W., Brudnik, U., Draus-Barini, J., Kupiec, T. & Wojas-Pelc, A.
815 Association of the SLC45A2 gene with physiological human hair colour variation.
816 *J Hum Genet* **53**, 966-971 (2008).
817 31. Streisinger, G., Singer, F., Walker, C., Knauber, D. & Dower, N. Segregation
818 analyses and gene-centromere distances in zebrafish. *Genetics* **112**, 311-9
819 (1986).
820 32. Weiss, J.M. *et al.* Anatomic position determines oncogenic specificity in
821 melanoma. *Nature* **604**, 354-361 (2022).
822 33. Hou, L., Arnheiter, H. & Pavan, W.J. Interspecies difference in the regulation of
823 melanocyte development by SOX10 and MITF. *Proc Natl Acad Sci U S A* **103**,
824 9081-5 (2006).

825 34. Kelsh, R.N. *et al.* Zebrafish pigmentation mutations and the processes of neural
826 crest development. *Development* **123**, 369-89 (1996).
827 35. Carney, T.J. *et al.* A direct role for Sox10 in specification of neural crest-derived
828 sensory neurons. *Development* **133**, 4619-30 (2006).
829 36. Cunningham, R.L. *et al.* Functional in vivo characterization of sox10 enhancers in
830 neural crest and melanoma development. *Commun Biol* **4**, 695 (2021).
831 37. Owen, J.P., Kelsh, R.N. & Yates, C.A. A quantitative modelling approach to
832 zebrafish pigment pattern formation. *Elife* **9**(2020).
833 38. Nagao, Y. *et al.* Distinct interactions of Sox5 and Sox10 in fate specification of
834 pigment cells in medaka and zebrafish. *PLoS Genet* **14**, e1007260 (2018).
835 39. O'Reilly-Pol, T. & Johnson, S.L. Neocuproine ablates melanocytes in adult
836 zebrafish. *Zebrafish* **5**, 257-64 (2008).
837 40. Cushion, T.D., Leca, I. & Keays, D.A. MAPping tubulin mutations. *Front Cell Dev*
838 *Biol* **11**, 1136699 (2023).
839 41. Rogers, S.L., Tint, I.S., Fanapour, P.C. & Gelfand, V.I. Regulated bidirectional
840 motility of melanophore pigment granules along microtubules in vitro. *Proc Natl*
841 *Acad Sci U S A* **94**, 3720-5 (1997).
842 42. Larson, T.A., Gordon, T.N., Lau, H.E. & Parichy, D.M. Defective adult
843 oligodendrocyte and Schwann cell development, pigment pattern, and
844 craniofacial morphology in puma mutant zebrafish having an alpha tubulin
845 mutation. *Dev Biol* **346**, 296-309 (2010).
846 43. Farnsworth, D.R., Saunders, L.M. & Miller, A.C. A single-cell transcriptome atlas
847 for zebrafish development. *Dev Biol* **459**, 100-108 (2020).
848 44. Neuhauss, S.C. *et al.* Genetic disorders of vision revealed by a behavioral screen
849 of 400 essential loci in zebrafish. *J Neurosci* **19**, 8603-15 (1999).
850 45. Myers, K.A., Bello-Espinosa, L.E., Kherani, A., Wei, X.C. & Innes, A.M. TUBA1A
851 Mutation Associated With Eye Abnormalities in Addition to Brain Malformation.
852 *Pediatr Neurol* **53**, 442-4 (2015).
853 46. Veldman, M.B., Bemben, M.A. & Goldman, D. Tuba1a gene expression is
854 regulated by KLF6/7 and is necessary for CNS development and regeneration in
855 zebrafish. *Mol Cell Neurosci* **43**, 370-83 (2010).
856 47. Roh, M.R. *et al.* Promoter Methylation of PTEN Is a Significant Prognostic Factor
857 in Melanoma Survival. *J Invest Dermatol* **136**, 1002-1011 (2016).
858 48. Palmieri, G. *et al.* Multiple Molecular Pathways in Melanomagenesis:
859 Characterization of Therapeutic Targets. *Front Oncol* **5**, 183 (2015).
860 49. Frantz, W.T. & Ceol, C.J. From Tank to Treatment: Modeling Melanoma in
861 Zebrafish. *Cells* **9**(2020).
862 50. Ignatius, M.S. *et al.* tp53 deficiency causes a wide tumor spectrum and increases
863 embryonal rhabdomyosarcoma metastasis in zebrafish. *Elife* **7**(2018).
864 51. Patton, E.E. *et al.* BRAF mutations are sufficient to promote nevi formation and
865 cooperate with p53 in the genesis of melanoma. *Curr Biol* **15**, 249-54 (2005).
866 52. He, S. *et al.* Synergistic melanoma cell death mediated by inhibition of both
867 MCL1 and BCL2 in high-risk tumors driven by NF1/PTEN loss. *Oncogene* **40**,
868 5718-5729 (2021).

869 53. Montal, E., Suresh, S., Ma, Y., Tagore, M.M. & White, R.M. Cancer Modeling by
870 Transgene Electroporation in Adult Zebrafish (TEAZ). *Methods Mol Biol* **2707**,
871 83-97 (2024).
872 54. Croushore, J.A. *et al.* Ptena and ptenb genes play distinct roles in zebrafish
873 embryogenesis. *Dev Dyn* **234**, 911-21 (2005).
874 55. Faucherre, A., Taylor, G.S., Overvoorde, J., Dixon, J.E. & Hertog, J. Zebrafish
875 pten genes have overlapping and non-redundant functions in tumorigenesis and
876 embryonic development. *Oncogene* **27**, 1079-86 (2008).
877 56. Kaufman, C.K. *et al.* A zebrafish melanoma model reveals emergence of neural
878 crest identity during melanoma initiation. *Science* **351**, aad2197 (2016).
879 57. Shakhova, O. *et al.* Antagonistic cross-regulation between Sox9 and Sox10
880 controls an anti-tumorigenic program in melanoma. *PLoS Genet* **11**, e1004877
881 (2015).
882 58. Hoek, K.S. *et al.* In vivo switching of human melanoma cells between proliferative
883 and invasive states. *Cancer Res* **68**, 650-6 (2008).
884 59. Solnica-Krezel, L., Schier, A.F. & Driever, W. Efficient recovery of ENU-induced
885 mutations from the zebrafish germline. *Genetics* **136**, 1401-20 (1994).
886 60. Russell, W.L. *et al.* Specific-locus test shows ethylnitrosourea to be the most
887 potent mutagen in the mouse. *Proc Natl Acad Sci U S A* **76**, 5818-9 (1979).
888 61. Cerami, E. *et al.* The cBio cancer genomics portal: an open platform for exploring
889 multidimensional cancer genomics data. *Cancer Discov* **2**, 401-4 (2012).
890 62. Alexandrov, L.B. *et al.* Signatures of mutational processes in human cancer.
891 *Nature* **500**, 415-21 (2013).
892 63. Cheng, P.F. *et al.* Methylation-dependent SOX9 expression mediates invasion in
893 human melanoma cells and is a negative prognostic factor in advanced
894 melanoma. *Genome Biol* **16**, 42 (2015).
895 64. Yang, X. *et al.* SOX9 is a dose-dependent metastatic fate determinant in
896 melanoma. *J Exp Clin Cancer Res* **38**, 17 (2019).
897 65. Hossain, S.M. & Eccles, M.R. Phenotype Switching and the Melanoma
898 Microenvironment; Impact on Immunotherapy and Drug Resistance. *Int J Mol Sci*
899 **24**(2023).
900 66. Travnickova, J. *et al.* Zebrafish MITF-Low Melanoma Subtype Models Reveal
901 Transcriptional Subclusters and MITF-Independent Residual Disease. *Cancer*
902 *Res* **79**, 5769-5784 (2019).
903 67. Weiss, J.M. *et al.* Shifting the focus of zebrafish toward a model of the tumor
904 microenvironment. *Elife* **11**(2022).
905 68. Sun, N. *et al.* Development of drug-inducible CRISPR-Cas9 systems for large-
906 scale functional screening. *BMC Genomics* **20**, 225 (2019).
907 69. Huang, Y. *et al.* CRISPR-dCas13-tracing reveals transcriptional memory and
908 limited mRNA export in developing zebrafish embryos. *Genome Biol* **24**, 15
909 (2023).
910 70. Kushawah, G. *et al.* CRISPR-Cas13d Induces Efficient mRNA Knockdown in
911 Animal Embryos. *Dev Cell* **54**, 805-817 e7 (2020).
912 71. Jao, L.E., Wente, S.R. & Chen, W. Efficient multiplex biallelic zebrafish genome
913 editing using a CRISPR nuclease system. *Proc Natl Acad Sci U S A* **110**, 13904-
914 9 (2013).

72. Ibarra-Garcia-Padilla, R., Howard, A.G.A.t., Singleton, E.W. & Uribe, R.A. A protocol for whole-mount immuno-coupled hybridization chain reaction (WICHCR) in zebrafish embryos and larvae. *STAR Protoc* **2**, 100709 (2021).
73. Suresh, S. *et al.* Identifying the Transcriptional Drivers of Metastasis Embedded within Localized Melanoma. *Cancer Discov* **13**, 194-215 (2023).
74. Labun, K. *et al.* CHOPCHOP v3: expanding the CRISPR web toolbox beyond genome editing. *Nucleic Acids Res* **47**, W171-W174 (2019).
75. Clement, K. *et al.* CRISPResso2 provides accurate and rapid genome editing sequence analysis. *Nat Biotechnol* **37**, 224-226 (2019).
76. Lindsay, H. *et al.* CrispRVariants charts the mutation spectrum of genome engineering experiments. *Nat Biotechnol* **34**, 701-2 (2016).
77. Stirling, D.R. *et al.* CellProfiler 4: improvements in speed, utility and usability. *BMC Bioinformatics* **22**, 433 (2021).
78. Hao, Y. *et al.* Dictionary learning for integrative, multimodal and scalable single-cell analysis. *Nat Biotechnol* **42**, 293-304 (2024).

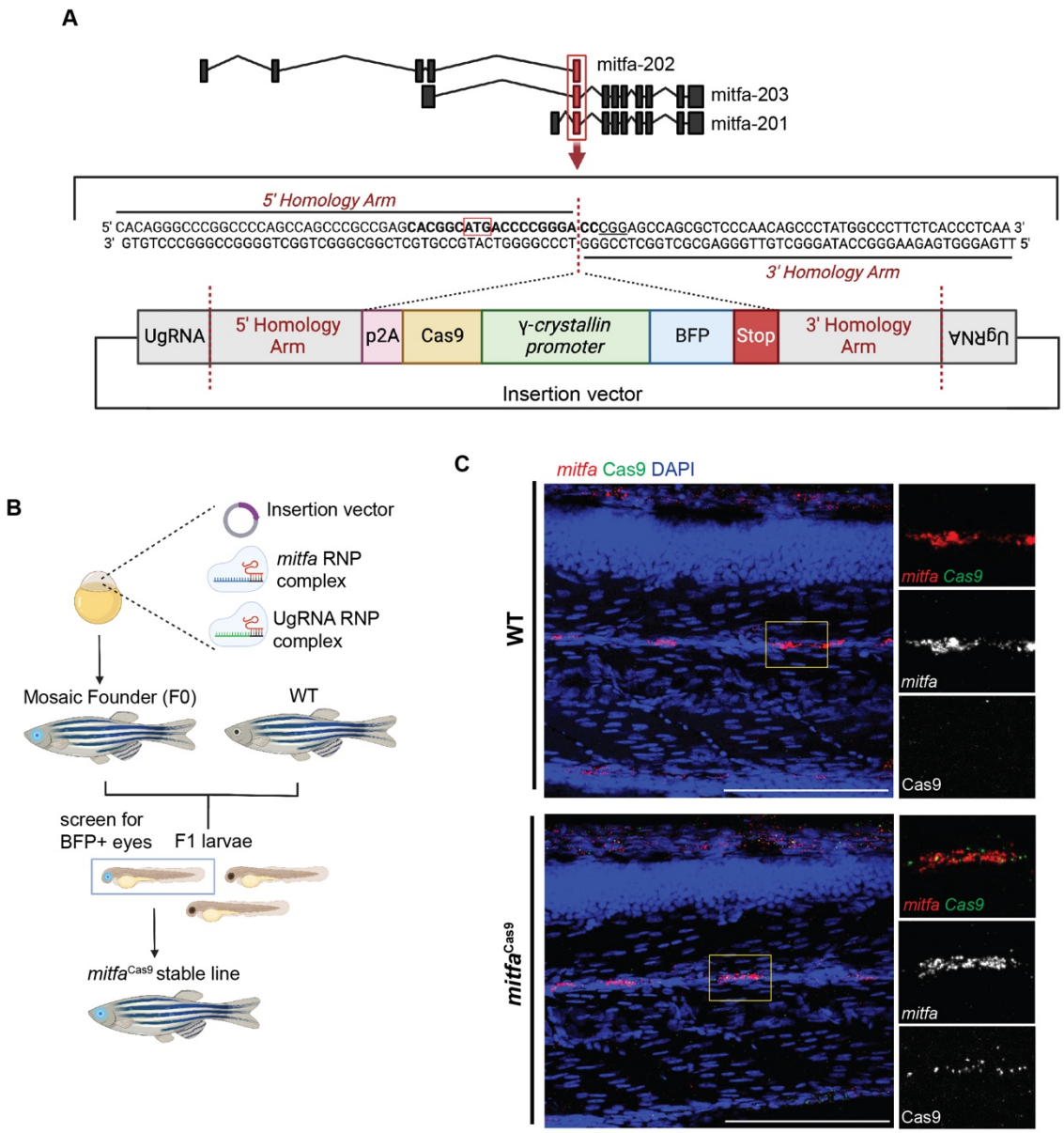

932

933 **Figure 1. Targeted integration of Cas9 to the *mitfa* locus with GeneWeld knockin system.**
934 **(A)** Schematic depicting integration site and GeneWeld knock-in cassette. 5' and 3' homology
935 arms are designed to target exon 2 of the zebrafish *mitfa* gene. The knock-in cassette includes
936 p2A followed by Cas9 and BFP driven by the eye-specific promoter gamma-crystallin. **(B)**
937 Pipeline to produce F1 mitfa^{Cas9} zebrafish. The GeneWeld knock-in vector and gRNAs targeting
938 the *mitfa* genomic insertion site or specific sites on the knock-in vector (UgRNA) are co-injected
939 into one-cell stage wild-type zebrafish embryos. Embryos are screened for BFP+ eyes marking
940 mosaic integration. These mosaic founder fish are then raised to adulthood and crossed with
941 wild-type fish. The resulting embryos are screened for BFP+ eyes and sequenced to confirm
942 precise integration. **(C)** Fluorescent in situ hybridization chain reaction (FISH) on 3dpf wild-type
943 and *mitfa*^{Cas9} embryos treated with 1-phenyl 2-thiourea (PTU). The presence of *mitfa* and Cas9
944 RNA was assessed by confocal microscopy at 40x magnification. Maximum intensity projections
945 are shown. n=17 WT embryos and n=16 mitfa^{Cas9} embryos were screened. Scale bars, 100μm.

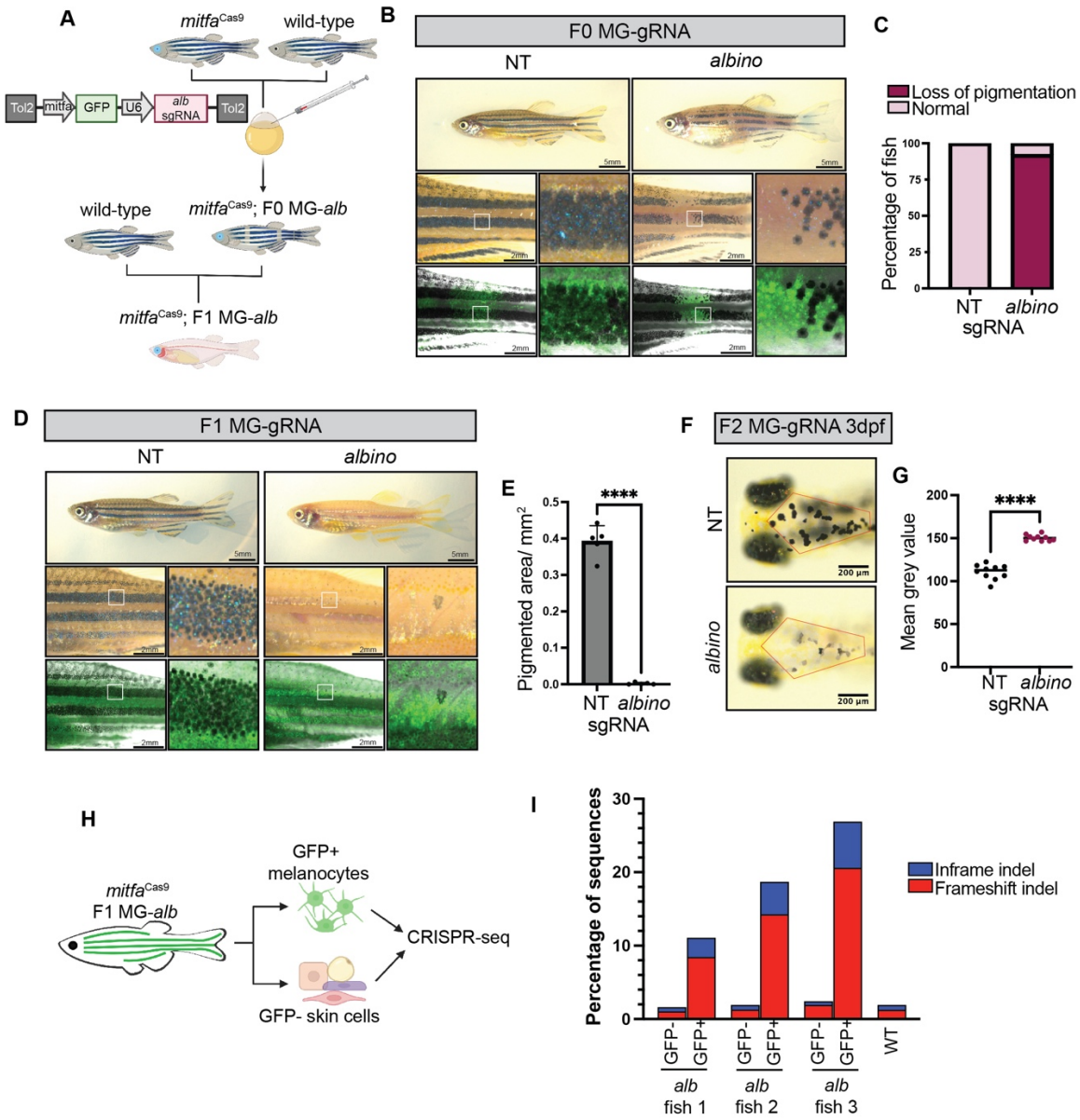

Figure 2. Melanocyte lineage-specific knockout of *albino* using *mitfa*^{Cas9} fish. **(A)** Pipeline to generate F0 and F1 *mitfa*:GFP;U6:gRNA (MG-gRNA) zebrafish. **(B)** Adult mitfa^{Cas9} MG-NT and MG-*albino* F0 fish. **(C)** Proportion of MG-NT (n=19) and MG-*albino* (n=25) F0 fish with loss of pigmentation phenotype. **(D)** Adult mitfa^{Cas9} MG-NT and MG-*albino* F1 fish. **(E)** Pigmented area/ mm^2 calculated for n=5 fish/ genotype within a defined rectangular region of interest (ROI) encompassing the top and middle melanocyte stripes. Two-sided student's *t*-test was used to assess statistical significance, **** $p < 0.0001$; error bars, SD. **(F)** 3dpf mitfa^{Cas9} MG-NT and MG-*albino* F2 fish. Representative embryos are shown for each genotype. **(G)** Mean grey value of head melanocytes calculated for n=10 embryos/genotype within a defined hexagonal ROI indicated as a red outline in 2F. Two-sided student's *t*-test was used to assess statistical significance, **** $p < 0.0001$. **(H)** Schematic for CRISPR sequencing protocol. **(I)** CRISPR-seq results are shown for WT and n=3 independent F1 MG-*albino* fish. Only GFP negative cells were isolated from WT fish. Results are shown as a fraction of sequences with indels calculated using CRISPRESSO.

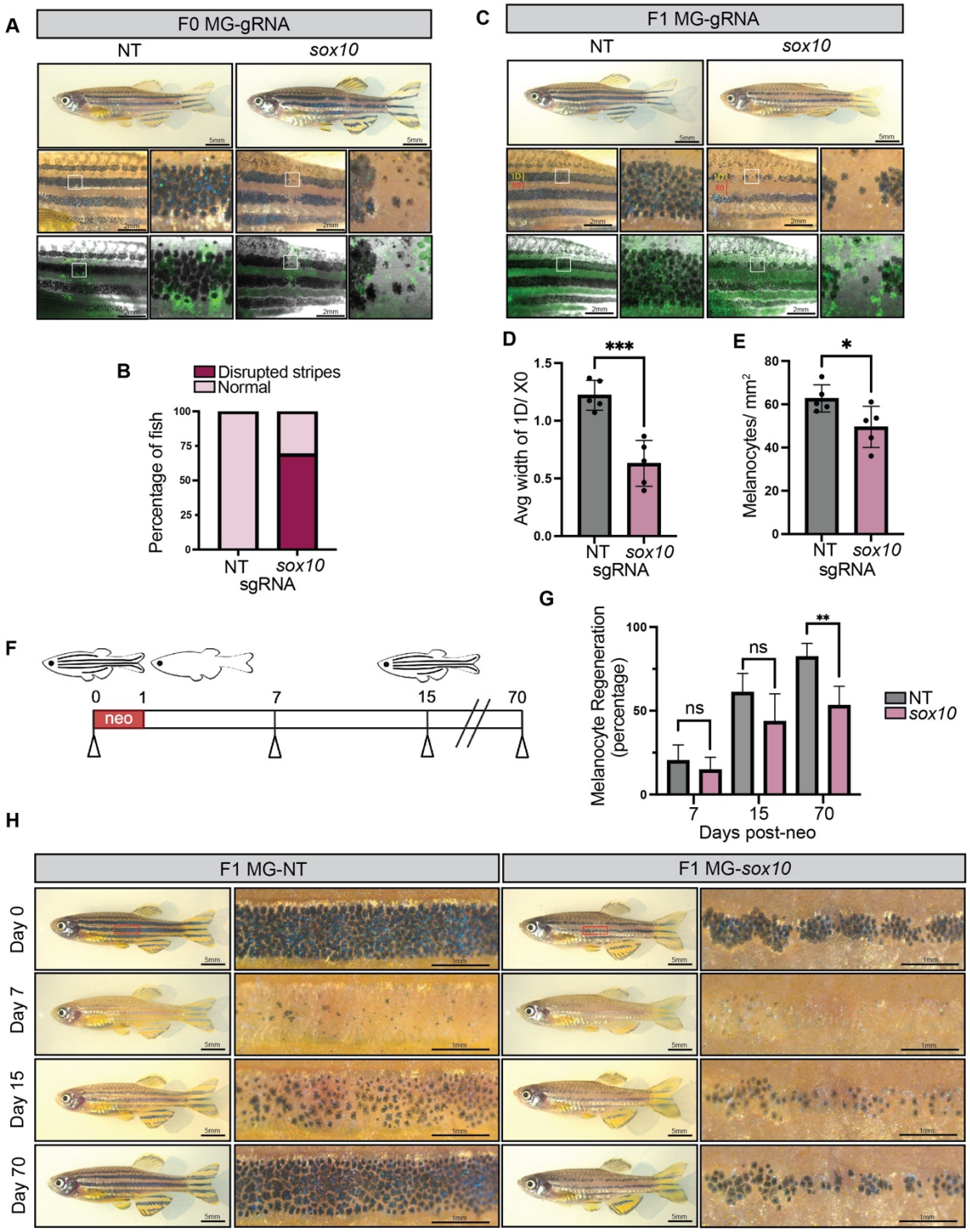

Figure 3. Melanocyte lineage-specific knockout of *sox10* using *mitfa*^{Cas9} fish. (A) Adult mitfa^{Cas9} MG-NT and MG-*sox10* F0 fish. **(B)** Proportion of MG-NT (n=19) and MG-*sox10* (n=16) F0 fish with disrupted stripes phenotype. **(C)** Adult mitfa^{Cas9} MG-NT and MG-*sox10* F1 fish. **(D)** The average width of melanocyte stripe 1D and xanthophore interstripe X0 was calculated for each fish by averaging 5 stripe/interstripe width measurements. N=5 fish per

967 genotype. Two-sided student's *t*-test was used to assess statistical significance, *** $p < 0.001$;
968 error bars, SD. **(E)** F1 MG-NT (n=5) and MG-*sox10* (n=5) adult fish were treated with
969 epinephrine and melanocytes were counted within a defined rectangular region of interest
970 3.46mm x 2.54mm encompassing the top and middle melanocyte stripes. Two-sided student's *t*-
971 test was used to assess statistical significance, * $p < 0.05$; error bars, SD. **(F)** Schematic of
972 neocuproine (neo) experimental setup. Adult mitfa^{Cas9} MG-NT (n= 5) and MG-*sox10* (n=5) F1
973 fish were treated with neocuproine for 24 hours to ablate melanocytes then imaged at day 7,15,
974 and 70 to measure regeneration of melanocytes compared to day 0. **(G)** Representative images
975 are shown for MG-NT and MG-*sox10* fish pre- and post-neocuproine treatment. **(H)**
976 Quantification of melanocyte regeneration. Fish were treated with epinephrine prior to imaging
977 to enable counting of melanocytes. Two-sided student's *t*-test was used to assess statistical
978 significance, ** $p < 0.01$; error bars, SD.
979
980

981
982
983
984

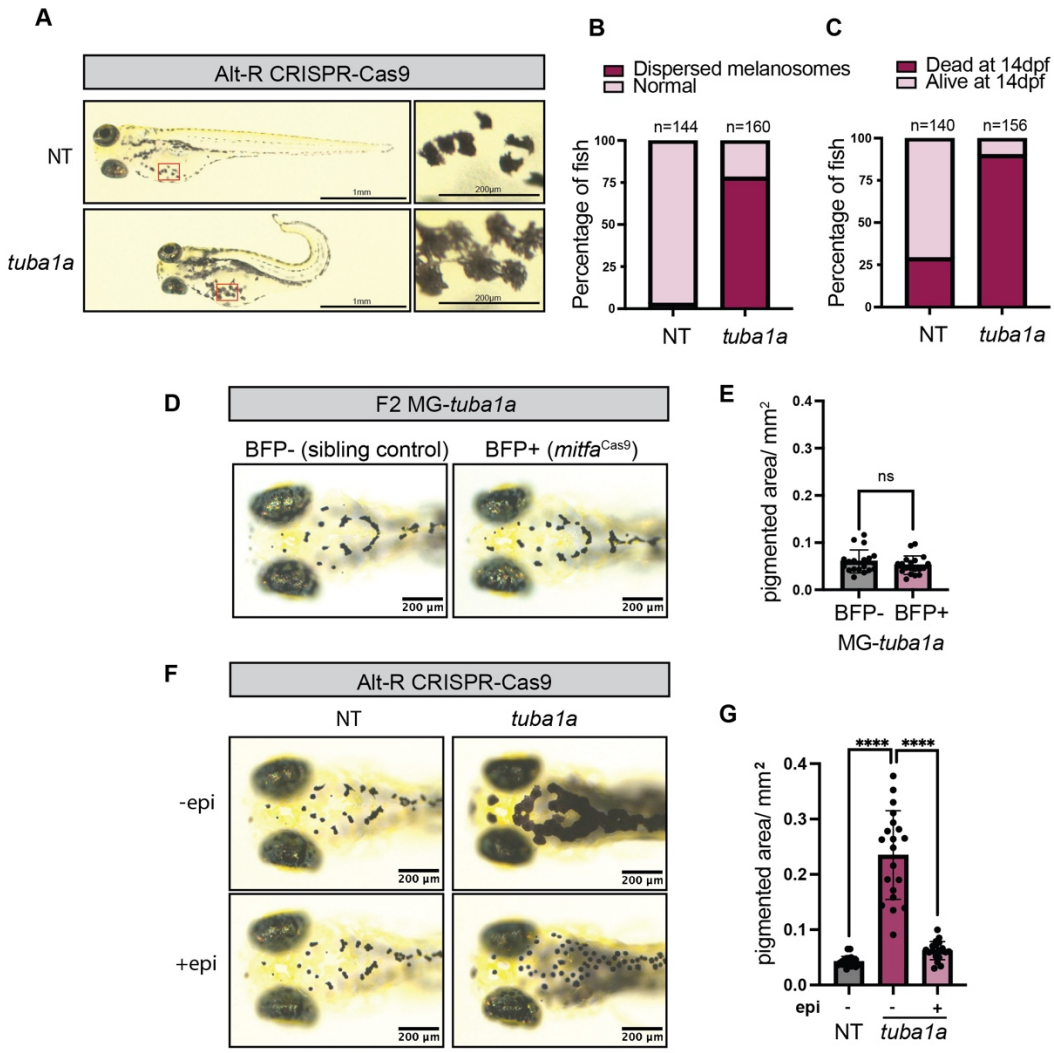

Figure 4. Non-autonomous function of *tuba1a* on melanocytes.
(A) 4dpf zebrafish embryos injected with either NT or *tuba1a* Alt-R CRISPR Cas9 gRNAs. **(B)** Percentage of NT or *tuba1a* Alt-R zebrafish embryos with dispersed melanocyte phenotypes. N=2 independent experiments. **(C)** Survival percentage is shown for NT and *tuba1a* Alt-R embryos. Embryos were counted at 24hpf and again at 14dpf to determine survival. **(D)** 4dpf mitfa^{Cas9} MG-*tuba1a* F2 embryos (BFP+ eyes) compared to sibling controls with no mitfa^{Cas9} (BFP- eyes). Representative embryos are shown for each genotype. **(E)** Pigmented area/ mm^2 calculated for n=19 embryos/genotype from two independent MG-*tuba1a* F2 clutches. Two-sided student's *t*-test was used to assess statistical significance, ns: no significance. **(F)** 4dpf Alt-R injected zebrafish embryos imaged before and after epinephrine (epi) treatment. **(G)** Pigmented area/ mm^2 calculated for n=20 embryos/genotype from two independent clutches. Two-sided student's *t*-test was used to assess statistical significance, **** $p < 0.0001$.

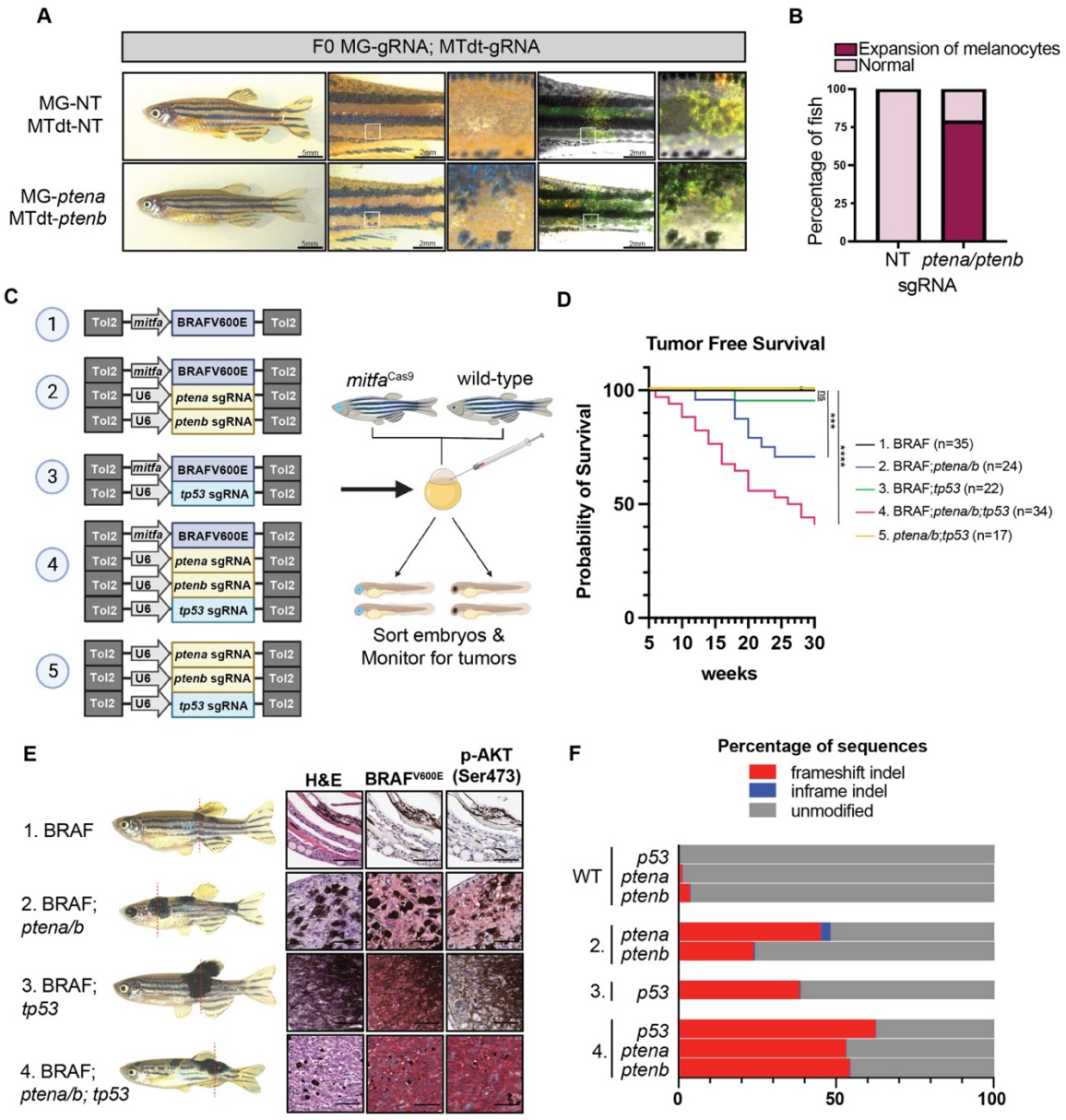

Figure 5. Generation of a zebrafish melanoma model in *mitfa*^{Cas9} fish.
(A) Adult mitfa^{Cas9} MG-NT; *mitfa*:TdT;U6:NT (MTdt-NT) and MG-*ptena*; MTdT-*ptenb* F0 fish. **(B)** Proportion of MG-NT; MTdT-NT (n=14) and MG-*ptena*; MTdT-*ptenb* (n=14) F0 fish with disrupted stripes phenotype. **(C)** Schematic of zebrafish tumorigenesis assay. Indicated plasmids are injected into one-cell stage embryos from crosses between mitfa^{Cas9} and WT fish. The mitfa:BRAF^{V600E} plasmid includes cardiac-specific cmlc2:GFP. Embryos were sorted for GFP+ hearts and BFP+ eyes and fish were screened every 2 weeks for tumors. **(D)** Tumor free survival curve. N=2 independent experiments. Tumors were tracked over the course of 30 weeks. Log-rank (Mantel-Cox) test was used to assess statistical significance, *** $p < 0.001$; **** $p < 0.0001$; ns: no significance. **(E)** Histology was performed on one fish from each indicated injection group. Dotted lines indicate site of sectioning. Red chromogen was used for all IHC staining. Scale bars, 50µm. **(F)** CRISPR-seq results are shown for normal skin dissected from WT fish and tumors dissected from injection conditions 2, 3, and 4. Results are shown as a fraction of sequences with indels calculated using CRISPRESSO.

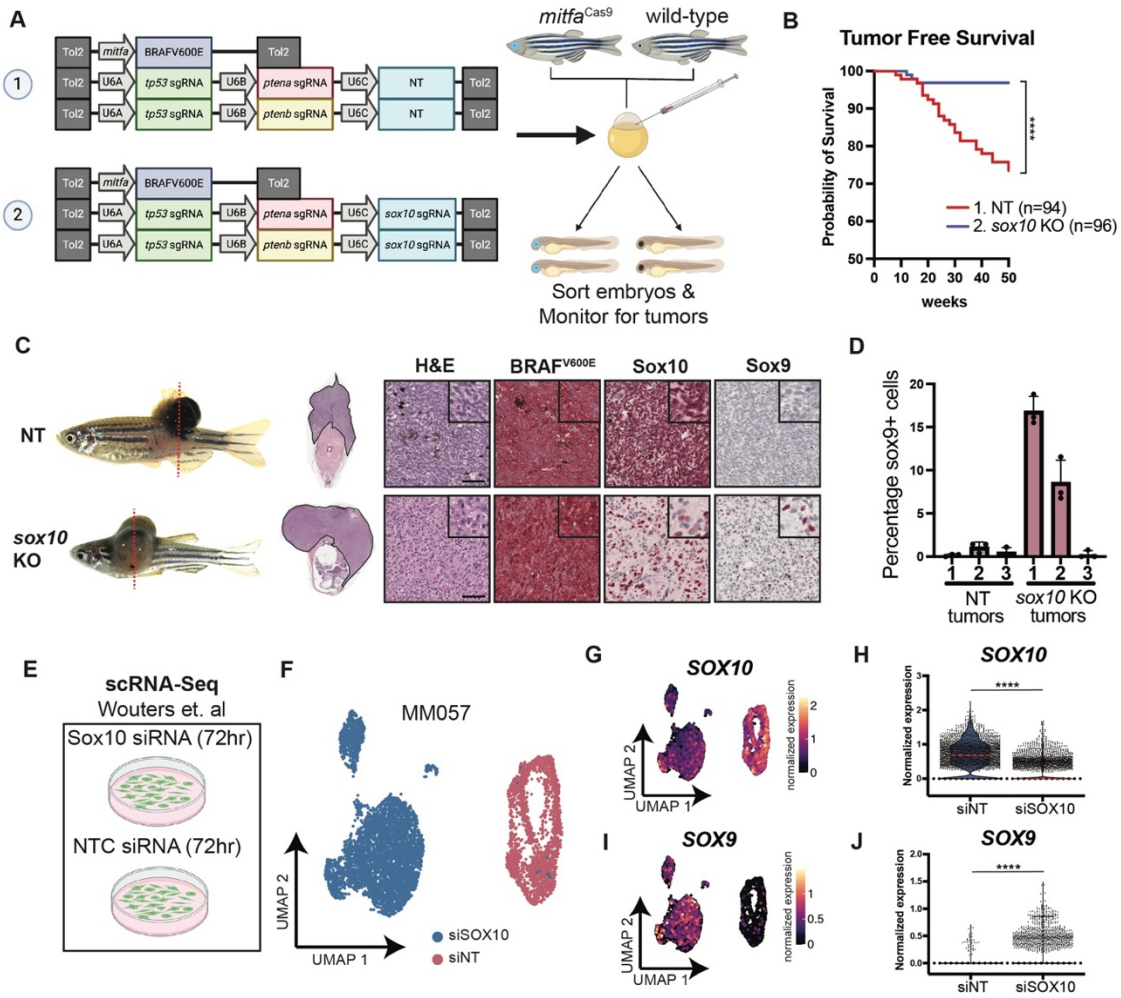

Figure 6. Melanoma specific knockout of *sox10* reduces tumor burden and induces phenotypic switching.

(A) Schematic of zebrafish tumorigenesis assay. Indicated plasmids are injected into one-cell stage embryos from crosses between mitfa^{Cas9} and WT fish. Embryos were sorted for GFP+ hearts and BFP+ eyes and fish were screened every 2 weeks for tumors. **(B)** Tumor free survival curve. N=3 independent experiments. Tumors were tracked over the course of 50 weeks. Log-rank (Mantel-Cox) test was used to assess statistical significance, **** $p < 0.0001$. **(C)** Histology is shown for one fish from each injection group. Dotted lines indicate site of sectioning. Red chromogen was used for all IHC staining. Scale bars, 50μm. **(D)** Color thresholding was used on IHC images to calculate the percentage of nuclei that stained positive for *sox9*. NT-1 n=1222 cells, NT-2 n=1620 cells, NT-3 n=2185 cells, sox10-1 n=970 cells, sox10-2 n=594, sox10-3 n=1046. Cells from n=3 images were analyzed for each tumor. **(E)** Schematic of scRNA-seq experimental setup from Wouters et al. Patient derived cell lines were treated with siRNAs targeting SOX10 or NTC and scRNA-seq was conducted at 72hrs. **(F)** UMAP of scRNA-seq dataset for MM057 cell line from Wouters et al. Cells from siSOX10 and siNT conditions are labeled. **(G)** Normalized expression of Sox10 per cell in UMAP space. **(H)** Violin plots of normalized expression of Sox10 per cell. Median is shown as dashed red line. Wilcoxon Rank Sum Test was used to assess statistical significance, **** $p < 0.0001$. **(I)** Normalized expression of Sox9 per cell in UMAP space. **(J)** Violin plots of normalized expression of Sox9 per cell. Wilcoxon Rank Sum Test was used to assess statistical significance, **** $p < 0.0001$.